

一种新型环氧化物水解酶的发现及其催化机理的阐明

朱美南^{1#}, 谷笑^{1#}, 柳得楷¹, 张凌志¹, 赵淑燕¹, 张礼娟², 张光亚¹, 江伟^{1*}

1 华侨大学 化工学院, 福建 厦门 361021

2 山东大学, 微生物技术国家重点实验室, 山东 青岛 266237

朱美南, 谷笑, 柳得楷, 张凌志, 赵淑燕, 张礼娟, 张光亚, 江伟. 一种新型环氧化物水解酶的发现及其催化机理的阐明[J]. 微生物学报, 2025, 65(1): 389-401.

ZHU Meinan, GU Xiao, LIU Dekai, ZHANG Lingzhi, ZHAO Shuyan, ZHANG Lijuan, ZHANG Guangya, JIANG Wei. Discovery of a novel epoxide hydrolase and elucidation of its catalytic mechanism[J]. Acta Microbiologica Sinica, 2025, 65(1): 389-401.

摘要:【目的】环氧化物水解酶(epoxide hydrolases, EHs)在手性药物的合成中起着重要作用。为了补充和发现更多的高性能环氧化物水解酶, 通过基因调取技术探索新的环氧化物水解酶。【方法】通过基因调取技术鉴定了一种来自卡尔斯巴德曲霉的新型环氧化物水解酶(*Aspergillus carlsbadensis* epoxide hydrolase, AcEH)。采用 AutoDock2 预测 AcEH 的关键水解位点, 通过计算设计阐明重要位点对 AcEH 的结构和催化机制的影响。【结果】对新型 AcEH 一级结构的分析揭示了 3 个特征性 α/β EH 基序的存在: HGWP、GYTFS 和 GGDIGS。AcEH 酶表现出高活性, 可在 15 min 内完全水解氧化苯乙烯(styrene oxide, SO), 比活性为 13 951 U/g。 K_m 、 V_{max} 和 k_{cat}/K_m 值分别为 (107.07±57.98) mmol/L、 (37.22±17.85) $\mu\text{mol}/(\text{min}\cdot\text{mg})$ 和 1.17 mmol/(L·s)。AcEH 的关键水解位点是催化三联体的 Asp192-His372-Glu346 和 2 个保守酪氨酸 Tyr251/314。某些突变(R49L、R49Y)导致酶失活, 而其他突变(Y45L)导致无活性包涵体的形成。相互作用网络分析显示, 第 49 个氨基酸残基的变化破坏了重要活性位点残基的相互作用, 导致酶失活。另一方面, 第 45 个氨基酸残基的改变使酶的结构不稳定, 导致包涵体的形成。【结论】本研究发现了一种新的环氧化物水解酶, 并分析了其水解机制, 为进一步研究这种酶及其工业化应用提供了有价值的见解。

资助项目: 国家自然科学基金(21808073); 福建省自然科学基金(2021J05058); 微生物技术开放项目国家重点实验室基金(M2022-02); 中央高校基本科研业务费专项资金(ZQN-814); 华侨大学高层次人才科研启动费(600005-Z17Y0072); 泉州市科技计划(2018C008)

This work was supported by the National Natural Science Foundation of China (21808073), the Natural Science Foundation of Fujian Province (2021J05058), the State Key Laboratory of Microbial Technology Open Projects Fund (M2022-02), the Fundamental Research Funds for the Central Universities (ZQN-814), the High-level Personnel Activation Fee of Huaqiao University (600005-Z17Y0072), and the Quanzhou City Science & Technology Program (2018C008).

[#]These authors contributed equally to this work.

*Corresponding author. E-mail: wjiang@hqu.edu.cn

Received: 2024-09-08; Accepted: 2024-11-02; Published online: 2024-11-06

关键词：生物催化；环氧化物水解酶；手性药物；分子动力学模拟；分子对接；水解机理

Discovery of a novel epoxide hydrolase and elucidation of its catalytic mechanism

ZHU Meinan^{1#}, GU Xiao^{1#}, LIU Dekai¹, ZHANG Lingzhi¹, ZHAO Shuyan¹, ZHANG Lijuan², ZHANG Guangya¹, JIANG Wei^{1*}

1 College of Chemical Engineering, Huaqiao University, Xiamen 361021, Fujian, China

2 State Key Laboratory of Microbial Technology, Shandong University, Qingdao 266237, Shandong, China

Abstract: [Objective] Epoxide hydrolases (EHs) play a key role in the synthesis of chiral pharmaceuticals. We explored new EHs by engineering or gene retrieval, aiming to enrich and discover more high-performance EHs. [Methods] A novel epoxide hydrolase (*Aspergillus carlsbadensis* epoxide hydrolase, AcEH) from *Aspergillus carlsbadensis* was identified by gene retrieval technology. We then used AutoDock2 to predict the key hydrolysis sites of AcEH and employed computational design to clarify the influences of important sites on the structure and catalytic mechanism of AcEH. [Results] The primary structure of the novel EH had three characteristic α/β EH motifs: HGWP, GYTFS, and GGDIGS. AcEH exhibited high activity and could completely hydrolyze styrene oxide (SO) within 15 min, with a specific activity of 13 951 U/g. The K_m , V_{max} , and k_{cat}/K_m of AcEH were (107.07 ± 57.98) mmol/L, (37.22 ± 17.85) $\mu\text{mol}/(\text{min}\cdot\text{mg})$, and 1.17 mmol/(L·s), respectively. The key hydrolysis sites of AcEH were Asp192-His372-Glu346, which catalyzed the triad, and two conserved tyrosine residues, Tyr251/314. The mutations R49L and R49Y caused enzyme inactivation, while the mutation Y45L resulted in the formation of inactive inclusion bodies. The interaction network revealed that changes in the 49th amino acid residue disrupted the interactions between key active site residues, leading to enzyme inactivation. On the other hand, the alteration of the 45th amino acid residue destabilized the enzyme structure, leading to the formation of inclusion bodies. [Conclusion] This study discovered a novel EH and analyzed its hydrolysis mechanism. The findings provide valuable insights for further research and engineering on this enzyme.

Keywords: biocatalysis; epoxide hydrolase; chiral pharmaceutical; molecular dynamics simulation; molecular docking; hydrolysis mechanism

Chiral epoxides and their adjacent diols play an important role in the fields of fine chemicals, materials and pharmaceuticals^[1]. They are valuable intermediates that can be used to synthesize important drugs and novel materials^[2-5]. For example, chiral epoxide

precursors can be used for the synthesis of important drugs and materials such as anti-obesity drugs (L-carnitine), anti-HIV drugs (lopinavir), calcium channel blockers (diltiazem), and chiral polyesters^[6-7]. (*R*)-octane-1,2-diol was used for the synthesis of mniopetal C, a

compound inhibiting the reverse transcriptase of HIV-1, and (*R*)-7-octene-1,2-diol for greensorone C having anticancer activity, and so on^[8-9]. Although most chiral drugs can be synthesized using chemical methods, there are many issues associated with these methods, such as expensive chiral ligands^[10], environmentally unfriendly metal catalysts, and harsh reaction conditions^[11-12]. In contrast, biocatalysts not only exhibit excellent catalytic performance but are also environmentally friendly^[13]. Therefore, biocatalysis is considered a promising alternative or complement to chemical catalysis.

Epoxide hydrolases (EHs) are widely distributed in animals, plants and microorganisms^[14]. As a class of biocatalysts that do not require cofactors, they can selectively hydrolyze chiral epoxides to synthesize chiral epoxides and vicinal diols^[15]. EHs can be classified into α/β -fold hydrolases, leukotriene A₄ hydrolases, and limonene 1,2-epoxide hydrolases based on their structural organization^[16]. The majority of characterized EHs belong to the α/β -hydrolase fold superfamily, which is

characterized by an α/β domain consisting of a β -sheet surrounded by a cluster of α -helices, and a cap domain that contains a variable cap-loop^[9]. The substrate binding pocket is located between the two aforementioned structural domains. Its hydrolytic function is carried out by a catalytic triad (Asp-His-Asp/Glu) and two Tyr residues, Figure 1 depicts the hydrolysis process of EH as summarized from previous studies and the analysis of this article. Firstly, the substrate enters the active pocket and forms hydrogen bonds with two tyrosines, aiding in ring opening. Then, aspartate performs a nucleophilic attack on the α or β carbon atom of the epoxide ring, forming an intermediate. Finally, the activated water molecule by histidine and aspartic acid interacts with the intermediate, ultimately leading to the formation of vicinal diols^[17-18]. Currently, with the advancement of genomics, an increasing number of epoxy hydrolases from various sources have been discovered. However, almost none of these enzymes exhibit satisfactory catalytic performance. Therefore, it is highly necessary to engineer or genetically explore new epoxy hydrolases^[19].

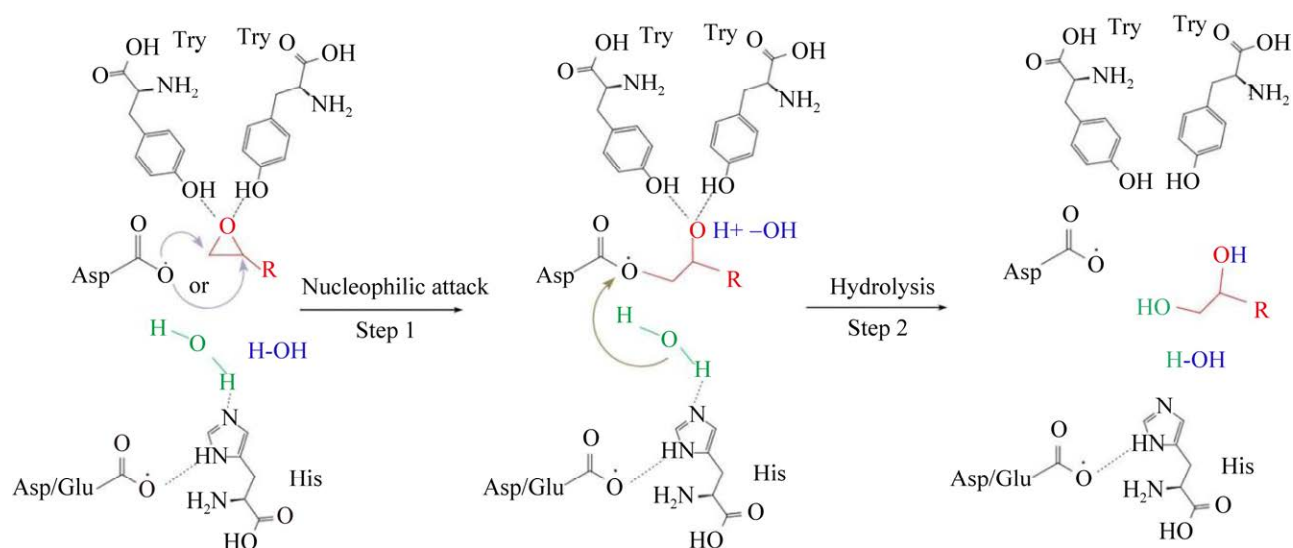


Figure 1 General hydrolysis steps of α/β -epoxide hydrolase. First step: Two conserved tyrosine residues form hydrogen bonds with the oxygen atom on the epoxide ring, stabilizing the binding between the epoxide substrate and the enzyme. An aspartic acid residue performs a nucleophilic attack on the epoxide ring, opening the ring and forming an intermediate. Second step: A water molecule activated by a histidine residue competitively attacks the intermediate, further opening it. The substrate is released, generating the corresponding vicinal diol product.

To supplement and discover more high-performance EHs, this study identified an enzyme (*Aspergillus carlsbadensis* epoxide hydrolase, AcEH) belonging to the α/β hydrolase family from *Aspergillus carlsbadensis*. The enzyme was successfully cloned and expressed in *Escherichia coli* BL21(DE3), demonstrating EH activity. The study then analyzed the basic enzymatic properties and hydrolysis mechanism. Additionally, during the process of modifying the thermal stability, two key sites were discovered that were of significant importance for enzyme activity and stability. Possible reasons for these findings were explored through analysis. The exceptional activity exhibited by AcEH suggests its potential as an industrial biocatalyst. Furthermore, the study of its hydrolysis mechanism and exploration of thermal stability modification can serve as a reference for future research.

1 Materials and Methods

1.1 Experimental materials

Escherichia coli DH5 α plasmid was cloned and heterologously expressed by BL21(DE3). They were purchased from Golden Bio Co. Ltd. (Golden Biotechnology Corporation, Beijing). AcEH was heterologously expressed with plasmid pET-28a. The original strains are kept in the laboratory. Kanamycin and IPTG were purchased from TaKaRa (TaKaRa Biomedical Technology Co., Ltd., Xiamen). The plasmid extraction kit and SDS-PAGE gel preparation kit were purchased from Omega (Omega Engineering). Other chemical reagents were purchased from Aladdin (Shanghai Aladdin Biochemical Technology Co., Ltd.) and were of chromatographic or analytical purity.

1.2 Database search and sequence analysis

Through gene retrieval on the NCBI server (<http://www.ncbi.nlm.nih.gov/>), protein sequences with homology lower than 80% to AnEH1 (CAB59813, PDB: 1QO7) and unknown function were searched. Unreported proteins were selected from these sequences, with homology ranging from 60% to 80%, for cloning and expression, aiming to discover new EHs. Furthermore, the

selected proteins were subjected to sequence alignment using the online tool ESPript 3.0 (<https://esprict.ibcp.fr/ESPript/ESPript/>). Subsequently, sequences from different *Aspergillus* species were selected, and the MEGA 11 software (<https://megasoftware.net/>) was used for processing and constructing a phylogenetic tree.

1.3 Cloning and expression of AcEH

The *E. coli* strain containing the EH gene was inoculated in LB medium supplemented with 100 $\mu\text{g}/\text{mL}$ kanamycin and incubated overnight at 37 °C as the seed culture. Subsequently, 2% (V/V) of the seed culture was inoculated into fresh LB medium and grown until reaching an OD_{600} of 0.6–0.8 at 37 °C. The culture was then induced with 0.1 mmol/L IPTG and incubated for 20 h at 18 °C. The cells were harvested, resuspended in a $\text{K}_2\text{HPO}_4\cdot\text{KH}_2\text{PO}_4$ buffer (100 mmol/L, pH 7.0), and subjected to sonication for disruption. The resulting mixture was centrifuged at 11 000 r/min for 30 minutes at 4 °C, and the supernatant was collected. The supernatant was filtered through a 0.22 μm membrane and purified using nickel Ni-NTA affinity chromatography to obtain the target protein enzyme as a catalyst.

1.4 Determination of protein and enzymatic properties

SDS-PAGE was used to analyze the expression of AcEH. Standard protein was used as a reference to estimate its apparent molecular weight using the ExpASY (<https://web.expasy.org/protparam/>) software. The concentration standard curves of SO, (S)-SO and (R)-SO, the activity of AcEH, pH stability, temperature stability and enzyme kinetics were determined using UV/Vis spectrophotometry with 4-(p-nitrobenzyl) pyridine (NBP) as previously described^[20-21]. Additionally, the effects of different metal ions and buffer solutions on enzyme activity were also measured.

To calculate the half-life of AcEH, the purified enzyme protein is incubated at 30 °C. Then, the enzyme activity of AcEH is measured at regular intervals using the untreated enzyme solution as a reference under optimal reaction conditions. The deactivation of AcEH follows a first-order kinetic model, and the formula to calculate the half-life is as follows formula (1).

$$K_c = \frac{2.0303}{t} \lg \frac{E_0}{E}$$

$$t_{1/2} = 0.693/K_c \quad (1)$$

In this context, K_c is the decay constant, E_0 represents the initial enzyme activity, while E represents the remaining enzyme activity at a given temperature (t).

The enzyme activity unit (U) is defined as the amount of enzyme required to consume 1 μ mol of substrate per minute under specified conditions. The specific enzyme activity (U/g) can be calculated using the formula (2).

Specific enzyme activity (U/g) = $C_0 \times v \times c / (t \times m)$ (2)
Where C_0 is the initial substrate concentration (20 mmol/L), v is the reaction volume, c is the substrate conversion rate, t is the reaction time (min), and m is the protein mass (g).

1.5 The hydrolysis mechanism of AcEH

Due to the low homology (64.12%) between the protein sequences of AcEH and the reported crystal structure (PDB ID: 1QO7), a combination of *de novo* modeling using AlphaFold2 (<https://alphafold.ebi.ac.uk/>) and homology modeling using SWISS-MODEL (<https://swissmodel.expasy.org/interactive>) is considered to predict its possible structure. Discovery Studio (DS2019) can be used for structural alignment and to evaluate its reliability using a Ramachandran plot (PyMOL: <https://pymol.org.edu/2/>). After obtaining the model, molecular docking of the protein-ligand complex can be performed using AutoDock (<http://www.autodock.scripps.edu>). The models with better overall scores can be selected to explain the hydrolysis mechanism of the enzyme. Finally, the results can be visualized using PyMOL. SO, (S)-SO, and (R)-SO ligands can be drawn using InDraw (<https://www.integle.com/static/indraw>). DS2019 originates from the servers of the Third Institute of Oceanography, Xiamen, Fujian.

1.6 Attempts to improve the thermal stability of AcEH

The modeling results of AcEH were input into FoldX (<https://foldxsuite.crg.eu/>) for comprehensive alanine scanning mutagenesis of its entire sequence, and the protein folding free

energy changes were calculated. Amino acid residues that had a detrimental effect on thermal stability were identified, and active pocket positions and conserved amino acids were filtered out. The remaining residues were subjected to amino acid saturation mutagenesis using I-Mutant 3.0 (<https://biofold.org/>) and FoldX. The selected variants from both methods were then input into GROMACS software (<https://www.gromacs.org/>) and Discovery Studio for molecular dynamics simulations and thermal stability analysis (Figures S2 and S3, Data has been submitted to the National Microbial Science Data Center, number: NMDCX0001726). Key mutants that significantly improved thermal stability were identified. Subsequently, primers were designed for the mutated primers (Table S1, Data has been submitted to the National Microbial Science Data Center, number: NMDCX0001726), and the mutations were verified by PCR amplification followed by 1% agarose gel electrophoresis. The PCR products were then digested overnight with *Dpn* I restriction enzyme. The PCR products were transformed into *Escherichia coli* DMT cells, and after incubation, plasmids were extracted and sent to a Sangon Biotechnology (Shanghai) Co., Ltd. The successfully sequenced plasmids were then transformed into *Escherichia coli* BL21(DE3) cells and stored in 30% glycerol.

2 Results and Discussion

2.1 Structure analysis of the AcEH

Through phylogenetic tree analysis, the result observed that the AcEH is distantly related to EH enzymes from other *Aspergillus* sources, indicating its novelty as an EH enzyme (Figure 2). Additionally, the amino acid sequence of AcEH shares more than 50% similarity with several EH enzymes from different *Aspergillus* sources (*AnEH1*, *AnEH2*, *AnEH3*, *AfEH*, *AfEH-Z5*, and *AfEH-293*). A sequence alignment was performed on these amino acids, and three characteristic regions were identified, as shown in Figure 2. Results revealed that AcEH contains a

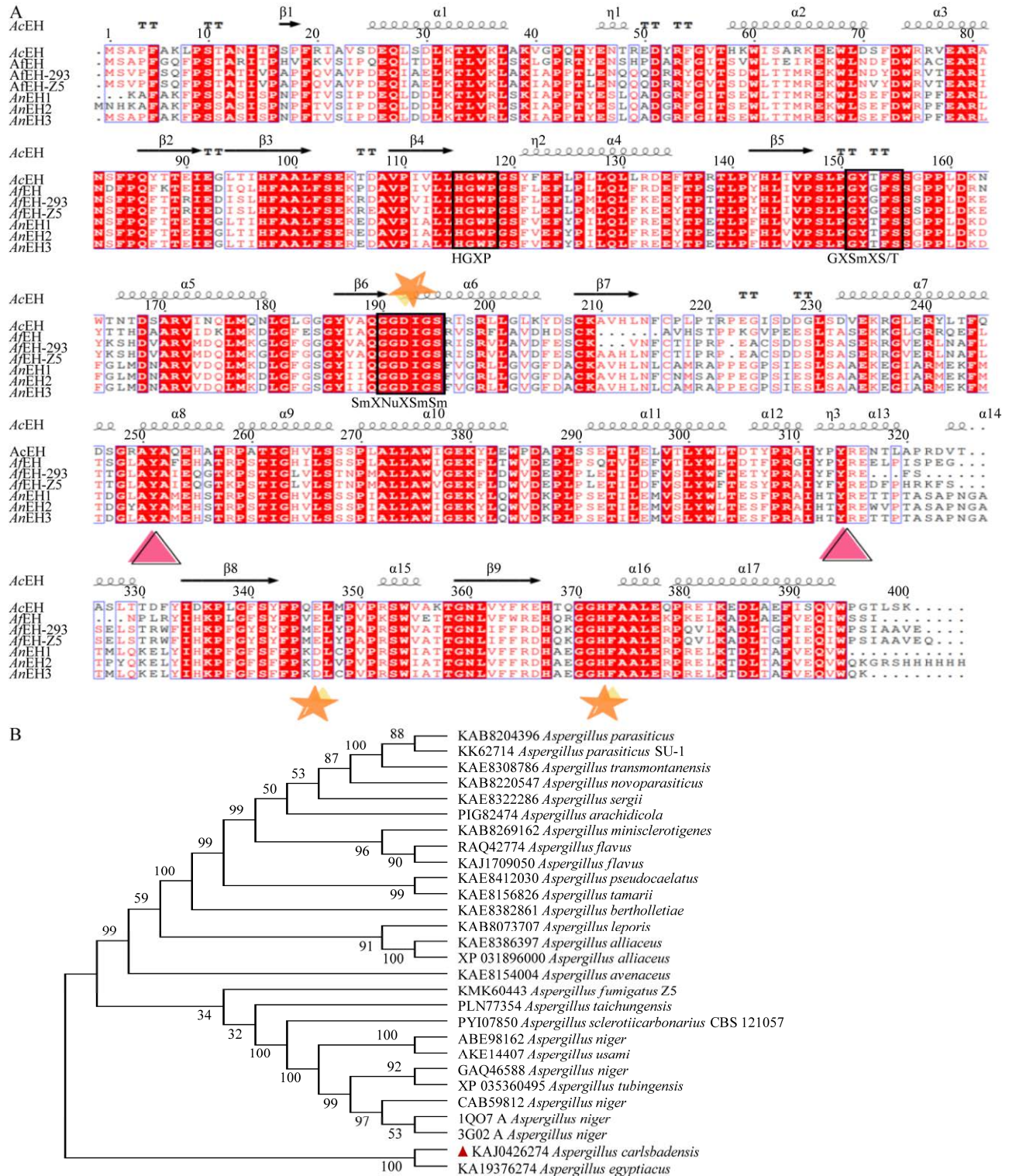


Figure 2 Multiple sequence alignment and phylogenetic tree of AcEH. A: Sequence alignment of AcEH with reported *Aspergillus* EHs. The black boxes indicate characteristic sequences of this type of enzyme, and the catalytic triad of AcEH is marked with orange pentagams (Asp¹⁹²-His³⁷²-Glu³⁴⁶), while the two conserved tyrosine residues (Tyr^{251/314}) are marked with pink triangles; B: Phylogenetic tree of AcEH, with the position of AcEH is indicated by red triangle.

characteristic region specific to α/β hydrolases^[22-23], namely SmXNuXSmSm (GGDIGS, amino acid position 190–195, where Sm, X, and Nu represent small amino acids, any amino acid, and nucleophilic amino acids, respectively), confirming its classification within the α/β hydrolase family. Furthermore, both AcEH and the aforementioned EHs share two conserved regions^[24]: the HGXP motif (HGWP, amino acid position 115–118), which has been shown to form an oxyanion hole stabilizing the anion formed during nucleophilic attack, and the GXSmXS/T motif (GYTFS, amino acid position 151–155). These findings indicate that the AcEH is an α/β EH.

2.2 Heterologous expression of the AcEH

By cloning and induced expression, it was discovered that only EH from *Aspergillus carlsbadensis* (referred to as AcEH) formed soluble expression. The purified protein of AcEH was obtained. The size of AcEH was analyzed using SDS-PAGE gel, and it has 400 amino acids in length. According to predictions from the ExpASY website, the estimated size of AcEH is around 41 kDa. Additionally, based on predictions from native PAGE, the non-denatured size and position of AcEH were larger than BSA (66 kDa). Considering that the template 1QO7 is a dimeric protein, it is speculated that AcEH may also be a dimeric protein (Figure S1, Data has been submitted to the National Microbial Science Data Center, number: NMDCX0001726).

2.3 Enzymatic properties of the AcEH

The enzymatic properties of the AcEH were determined, and the results are shown in Figure 3 and Table 1. Figure 3A indicates that the optimal pH for enzyme activity is 7.0, and the enzyme remains stable within the pH range of 6.0–7.5. Figure 3B demonstrates that the enzyme exhibits high activity at temperatures of 20–30 °C. In Figure 3C, it is observed that the enzyme remains stable when incubated at temperatures between 20 to 35 °C for 5 h, with enzyme activity maintained at over 80%. While the enzymatic reaction conditions of AcEH demand mild conditions, it exhibits remarkable stability, thereby conferring a distinct advantage in comparison to other

counterparts^[25-27]. Figure 3D shows that the majority of metal ions significantly inhibit the enzyme activity, except for Ca^{2+} at a concentration of 50 mg/L, which enhances the enzyme activity. Under optimal conditions, with SO as the substrate, AcEH has a half-life of 136.5 h. This is significantly higher than the reported EHs^[28-29]. In a 15 min reaction, it can achieve a maximum specific activity of 13 952 U/g, and it is capable of completely hydrolyzing both (*S*)-SO and (*R*)-SO. Its hydrolytic activity exhibits a substantial advantage compared to the reported EHs^[30].

The enzymatic kinetic parameters, as shown in Table 1, reveal that the enzyme exhibits excellent enzymatic activity and fast reaction rates towards SO, (*S*)-SO, and (*R*)-SO. The V_{\max} values are (37.22±17.85), (137.91±7.00), and (185.28±20.24) $\mu\text{mol}/(\text{min}\cdot\text{mg})$, respectively, which are significantly higher than those reported for EHs^[31]. Additionally, AcEH demonstrates high substrate affinity for both (*S*)- and (*R*)-configurations, with K_m values of (4.00±0.65) and (6.87±1.58) mmol/L, respectively. Unlike most EHs discovered so far, AcEH exhibits the ability to rapidly hydrolyze both enantiomers of chiral epoxides^[32-34], indicating its potential for enantioselective hydrolysis to produce pure racemic epoxides.

2.4 Hydrolysis mechanism of the AcEH

The results of the comparative analysis between the *de novo* modeling by AlphaFold and the homology modeling by SWISS-MODEL are shown in Figure 4A, with an RMSD (root mean square deviation) value of 0.530. This indicates a high similarity between the two modeling results. The Ramachandran plots evaluation of the two modeling results shows that 91.5% and 92.4% of the amino acids are located in the most favoured regions (Figure 4B). Generally, if more than 90.0% of the amino acid residues fall within the allowed and generously allowed regions, it can be considered that the conformation complies with the rules of stereochemistry^[35]. Therefore, the 3D structure of AcEH is considered reasonable and can be further analyzed.

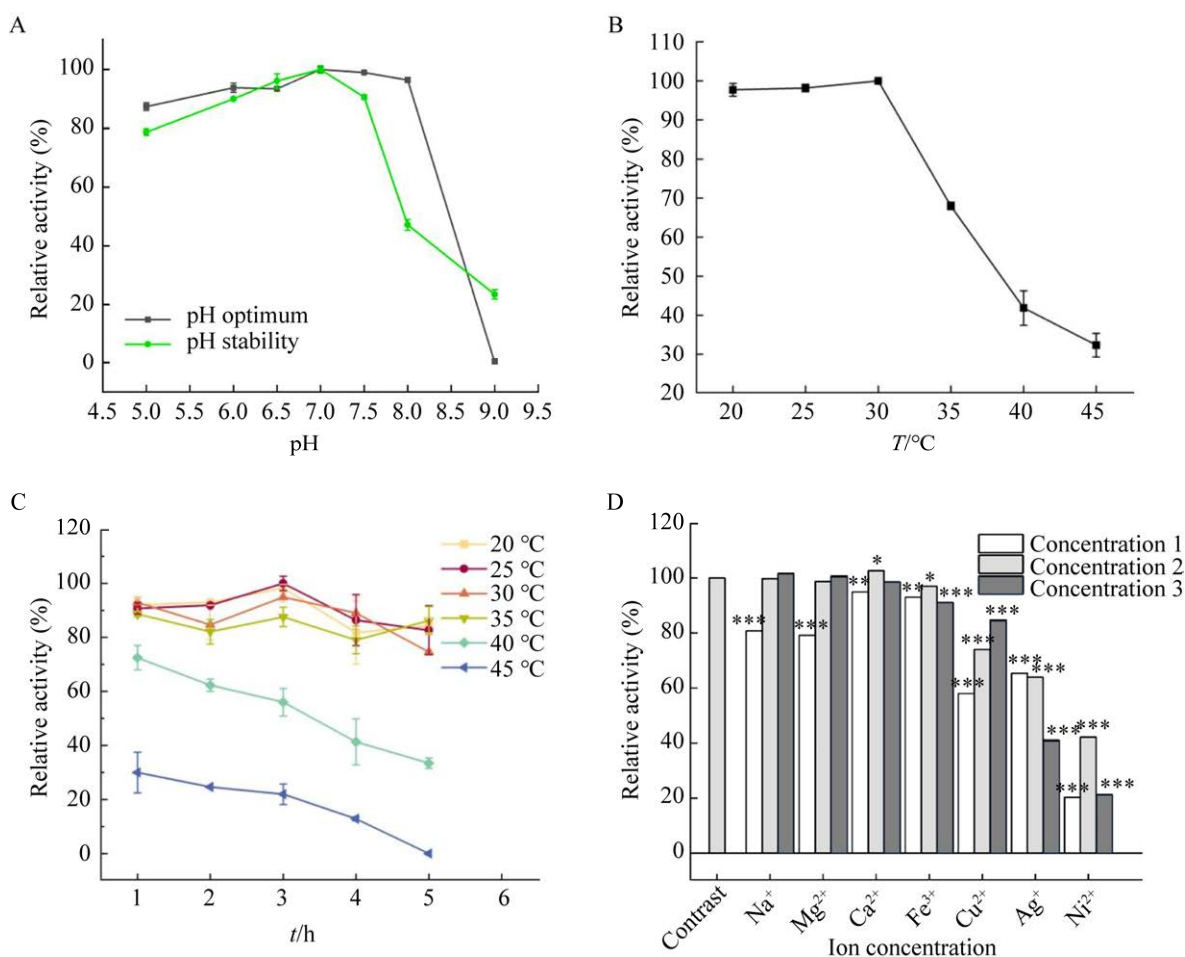


Figure 3 Factors influencing AcEH enzyme activity. A: Optimal reaction pH and pH stability within 1 h for AcEH; B: Optimal reaction temperature; C: Temperature stability within 5 h; D: Effect of different concentrations of metal ions on AcEH enzyme activity. Na⁺, Concentration 1: 0.87 mmol/L, Concentration 2: 2.17 mmol/L, Concentration 3: 4.35 mmol/L; Mg²⁺, Concentration 1: 0.83 mmol/L, Concentration 2: 2.08 mmol/L, Concentration 3: 4.16 mmol/L; Ca²⁺, Concentration 1: 0.50 mmol/L, Concentration 2: 1.25 mmol/L, Concentration 3: 2.50 mmol/L; Fe³⁺, Concentration 1: 0.36 mmol/L, Concentration 2: 0.89 mmol/L, Concentration 3: 1.79 mmol/L; Cu²⁺, Concentration 1: 0.31 mmol/L, Concentration 2: 0.78 mmol/L, Concentration 3: 1.56 mmol/L; Ag⁺, Concentration 1: 0.19 mmol/L, Concentration 2: 0.46 mmol/L, Concentration 3: 0.93 mmol/L; Ni²⁺, Concentration 1: 0.34 mmol/L, Concentration 2: 0.85 mmol/L, Concentration 3: 1.70 mmol/L. * $P \leq 0.05$, ** $P < 0.01$, *** $P < 0.001$ in comparison with contrast group.

Table 1 The kinetic constants of AcEH for substrates SO, (S)-SO, and (R)-SO

Substrate	K_m (mmol/L)	V_{max} ($\mu\text{mol}/(\text{min} \cdot \text{mg})$)	k_{cat} (s^{-1})	k_{cat}/K_m (mmol/(L·s))
SO	107.07±57.98	37.22±17.85	124.90±59.90	1.17
(S)-SO	4.00±0.65	137.91±7.00	331.04±16.80	82.76
(R)-SO	6.87±1.58	185.28±20.24	382.34±41.77	55.65

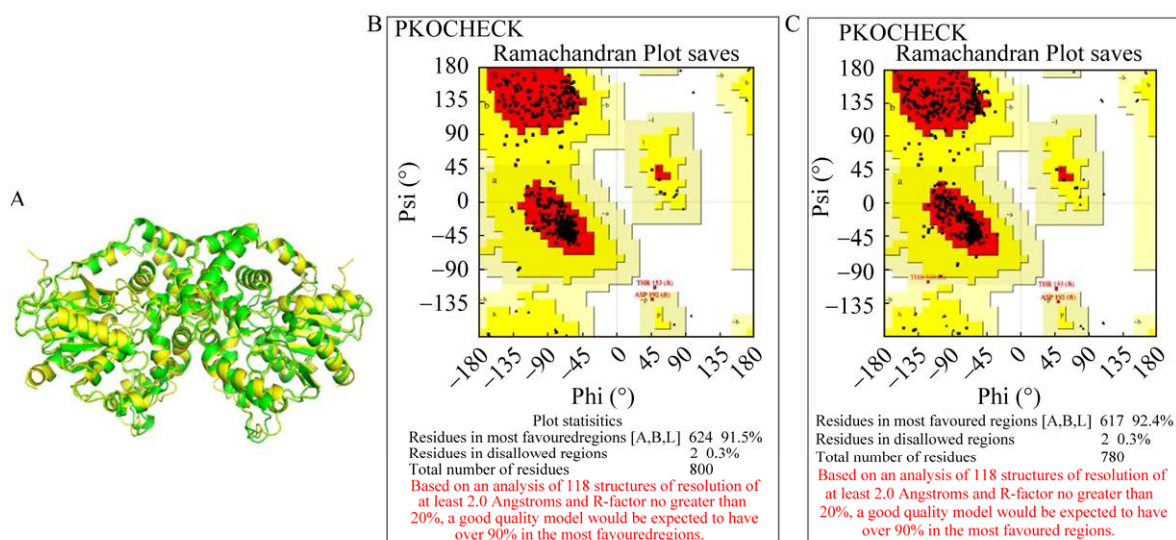


Figure 4 Three-dimensional structural prediction of *AcEH*. A: Alignment of AlphaFold *de novo* modeling (yellow) and SWISS-MODEL homology modeling (green), DMSO=0.530; B: Ramachandran plot evaluation of AlphaFold modeling results (91.5%); C: Ramachandran plot evaluation of SWISS-MODEL modeling results (92.4%).

The molecular docking of the protein-ligand complex was performed using AutoDock2, and the model with a better overall score was selected to explain the hydrolysis mechanism of the enzyme^[17]. The results are shown in Figure 5. Figure 5A depicts the 3D structure of the *AcEH* monomer, with the alpha helices shown in cyan, beta sheets in purple, loops in pink, and the solvent-accessible surface of the active pocket of *AcEH* in white. The green substance inside represents the SO. Figures 5B and 5C provide detailed views of the active pocket and the catalytic mechanism. The active pocket includes the classical catalytic triad (Asp¹⁹²-His³⁷²-Glu³⁴⁶) and two conserved tyrosine residues (Tyr²⁵¹, Tyr³¹⁴). The hydrolysis mechanism is consistent with the previously reported typical hydrolysis pathway. It is speculated that the hydrolysis steps inferred and summarized in Figure 1 are consistent with the hydrolysis steps mentioned: the active hydroxyl groups of the two Tyr^{251/314} residues form hydrogen bonds with the oxygen atoms in the epoxide ring, stabilizing the substrate. Simultaneously, the negatively charged Asp¹⁹² selectively nucleophilically attacks the two

carbon atoms in the epoxide ring. Then, a water molecule activated by histidine also nucleophilically attacks the substrate, opening the three-membered ring to form a tetrahedral intermediate. Finally, a water molecule donates a proton to release the resulting vicinal diol from the active site, completing the hydrolysis process.

2.5 Single point mutation modification and further mechanism exploration

After calculations, two optimal theoretical mutation sites were identified, namely position 45 and position 49. A total of three mutant variants were constructed, namely Y45L, R49L, and R49Y. The results revealed that the mutation at position 45 resulted in the formation of an inclusion body with no enzymatic activity, while the mutation at position 49 led to soluble expression of the enzyme but loss of enzymatic activity. Based on these findings, protein-protein interaction network analysis (PPI) of single-point mutants was carried out using the RING (Regulation of Interaction Networks in Genomes: <https://ring.biocomputingup.it/help>) website tool and Cytoscape to elucidate potential reasons^[36].

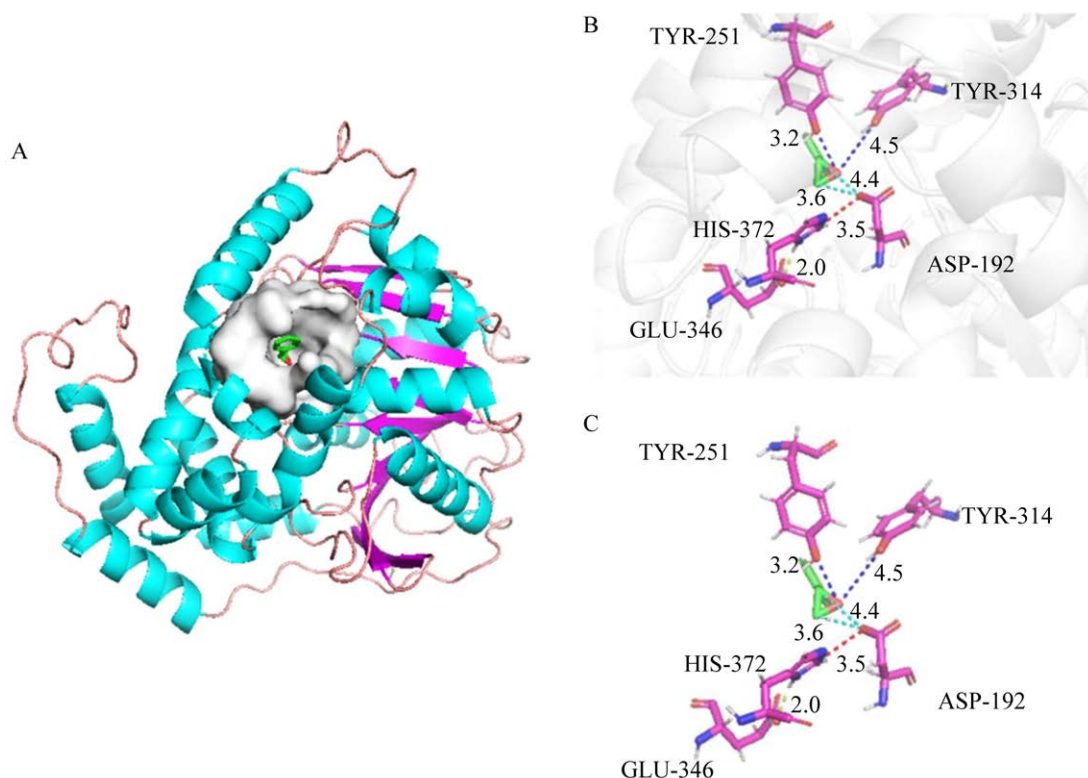


Figure 5 Presenting the 3D structure and hydrolytic mechanism of AcEH. A: The overall structure of AcEH with the active site labeled. The α -fold is depicted in light blue, the β -fold in purple, the connecting loop in pink, and the white surface represents the location of the active pocket. The green color represents the substrate SO, and the red color represents the oxygen atom in the epoxide ring. B–C: Local and detailed depiction of the interactions between the catalytic triad and the substrate.

Upon analysis, it was found that in the wild-type PPI as shown in Figure 6A, the key amino acids involved in the interaction of the wild-type protein are Trp²⁸⁴, His²⁵⁵, Tyr^{307/251}, Trp¹¹⁷, and Phe¹⁵⁴. In the Y45L mutant, as depicted in Figure 6B, the interaction between key amino acids Trp¹¹⁷ and Tyr²⁵¹ is reduced. By comparing the degree values of key sites in the wild-type and Y45L mutant, as shown in Table 2, it was observed that the degree value of the Tyr⁴⁵ node in the Y45L mutant is zero, indicating the complete disappearance of interactions with other amino acids. Protein structure analysis revealed that Tyr⁴⁵ is located on a loop in the AcEH protein folding structure. It is speculated that Tyr⁴⁵ on the loop plays a vital role in connecting the two α -helices, leading to the formation of inactive

inclusion body enzyme in the Y45L mutant. In the PPI of the R49L and R49Y mutant variants, shown in Figures 6C and 6D, the key amino acid interactions have also changed. Since both mutants lack enzymatic activity, the main analysis focused on the changes in the degree values of their interactions with the wild-type catalytic site. The results, as shown in Table 3, revealed a decrease of one degree value for each of the catalytic triad Asp¹⁹²-His³⁷²-Glu³⁴⁶, including the disappearance of the Ionic bond between Glu³⁴⁶ and His³⁷². It is speculated that this may be the main reason for the loss of enzyme activity, as the hydrolytic action of the enzyme requires the joint action of Glu³⁴⁶-His³⁷² to activate the water molecule for nucleophilic attack and proton transfer in the three-membered ring opening.

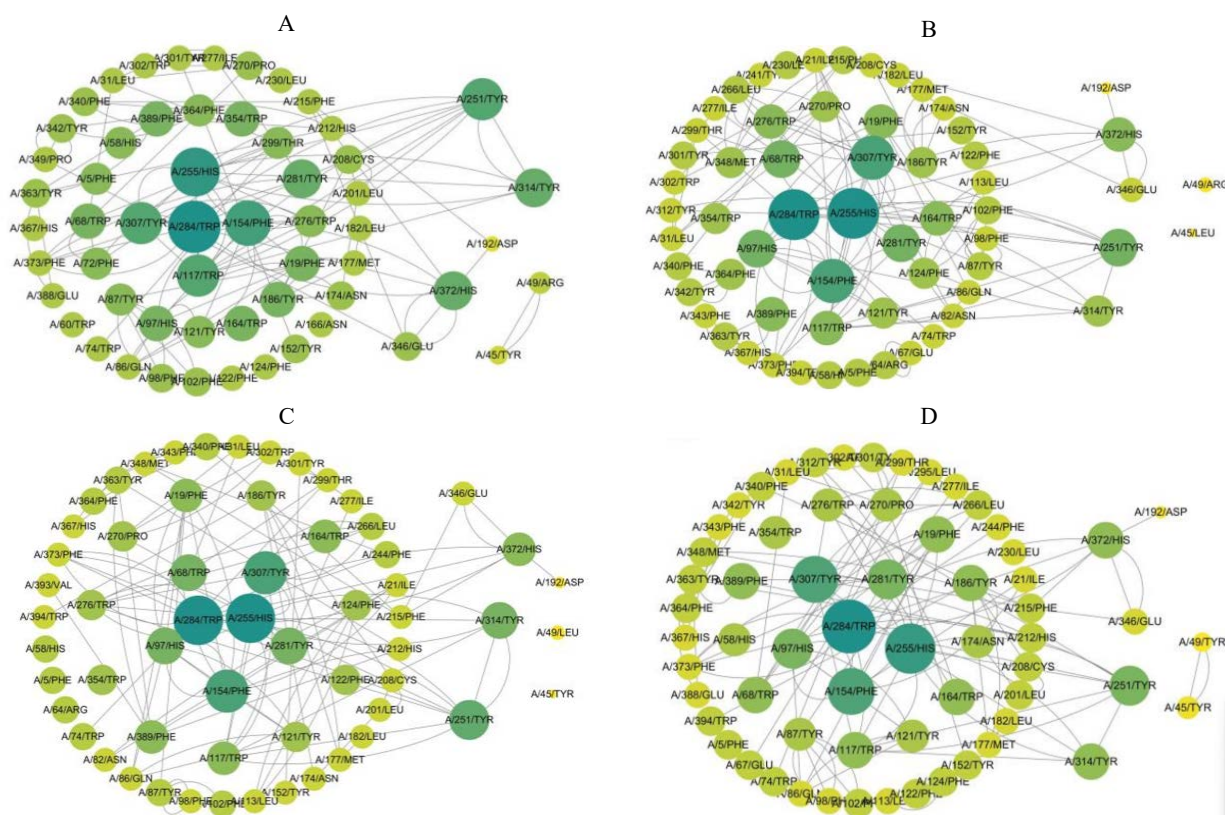


Figure 6 Protein-protein interaction network of wild-type, Y45L, R49L, and R49Y mutant variants. A: Wild-type; B: Y45L; C: R49L; D: R49Y.

Table 2 Degree values of key interaction sites between wild-type and mutant Y45L

Type	284	255	154	307	117	251	45	49
Wild-type	13	12	11	10	10	10	3	4
Y45L	13	13	11	11	8	9	0	2

Table 3 Degree values of the active sites of wild-type and mutant Y45L, R49L, R49Y

Type	192	372	346	251	314
Wild-type	2	9	6	10	9
Y45L	1	8	5	9	7
R49L	1	8	5	8	9
R49Y	1	8	5	10	9

3 Conclusion

In this study, AcEH was extracted by gene extraction and successfully expressed in *E. coli*. A new EH with high hydrolytic activity, long

half-life and enantiomeric hydrolysis was successfully found. At the same time, its hydrolysis principle was explained by bioinformatics technology, which provided a theoretical basis for the further study of the hydrolysis mechanism of the enzyme.

This study also constructed three mutants, although failed to achieve the expected results, but explained the possible reasons, but also provided some warnings and references for the transformation of the enzyme. The completion of this task is of great significance for further optimization and industrial application of AcEH.

Credit Authorship Contribution Statement

ZHU Meinan and GU Xiao: Conceptualization, Methodology, Data curation, Writing-original draft; LIU Dekai: Modeling,

molecular docking, Writing-review & editing; ZHANG Lingzhi: Dynamics simulation, Writing-review & editing; ZHAO Shuyan: Validation, Writing-review & editing; ZHANG Lijuan: Validation; ZHANG Guangya: Visualization, Writing-review & editing; JIANG Wei: Writing-review & editing.

Declaration of Competing Interest

The authors declare no competing financial interest.

Supplemental Information

Supplementary information has been submitted to the National Microbiological Science Data Center, number: NMDCX0001726.

References

- [1] HWANG S, CHOI YC, LEE YE. Bio- and chemo-catalytic preparations of chiral epoxides[J]. *Journal of Industrial and Engineering Chemistry*, 2010, 16(1): 1-6.
- [2] DUAN M, DÍAZ-OVIEDO CD, ZHOU Y, CHEN XY, YU PY, LIST B, HOUK KN, LAN Y. Chiral phosphoric acid catalyzed conversion of epoxides into thiiranes: mechanism, stereochemical model, and new catalyst design[J]. *Angewandte Chemie International Edition*, 2022, 61(9): e202113204.
- [3] LI J, LIU Y, REN WM, LU XB. Enantioselective terpolymerization of racemic and *meso*-epoxides with anhydrides for preparation of chiral polyesters[J]. *Proceedings of the National Academy of Sciences of the United States of America*, 2020, 117(27): 15429-15436.
- [4] HU FL, CHEN ZL, TAN Y, XU D, HUANG SL, JIA SQ, GONG XN, QIN WL, YAN HL. Organocatalytic enantioselective γ -elimination: applications in the preparation of chiral peroxides and epoxides[J]. *Organic Letters*, 2020, 22(5): 1934-1940.
- [5] LI J, REN BH, WAN ZQ, CHEN SY, LIU Y, REN WM, LU XB. Enantioselective resolution copolymerization of racemic epoxides and anhydrides: efficient approach for stereoregular polyesters and chiral epoxides[J]. *Journal of the American Chemical Society*, 2019, 141(22): 8937-8942.
- [6] MOSCHONA F, SAVVOPOULOU I, TSITOPPOULOU M, TATARAKI D, RASSIAS G. Epoxide syntheses and ring-opening reactions in drug development[J]. *Catalysts*, 2020, 10(10): 1117.
- [7] YANG H, YU HX, STOLARZEWICZ IA, TANG WJ. Enantioselective transformations in the synthesis of therapeutic agents[J]. *Chemical Reviews*, 2023, 123(15): 9397-9446.
- [8] MAYNERT EW, FOREMAN RL, WATABE T. Epoxides as obligatory intermediates in the metabolism of olefins to glycols[J]. *The Journal of Biological Chemistry*, 1970, 245(20): 5234-5238.
- [9] HU B, HU D, ZHANG D, WEN Z, ZANG J, WU MC. Manipulating the regioselectivity of a *Solanum lycopersicum* epoxide hydrolase for the enantioconvergent synthesis of enantiopure alkane- and alkene-1,2-diols[J]. *Catalysis Science & Technology*, 2020, 10(17): 5886-5895.
- [10] JIANG JJ, WONG MK. Recent advances in the development of chiral gold complexes for catalytic asymmetric catalysis[J]. *Chemistry-An Asian Journal*, 2021, 16(5): 364-377.
- [11] ETAYO P, VIDAL-FERRAN A. Rhodium-catalysed asymmetric hydrogenation as a valuable synthetic tool for the preparation of chiral drugs[J]. *Chemical Society Reviews*, 2013, 42(2): 728-54.
- [12] YOON M, SRIRAMBALAJI R, KIM K. Homochiral metal-organic frameworks for asymmetric heterogeneous catalysis[J]. *Chemical Reviews*, 2012, 112(2): 1196-1231.
- [13] ROSSINO G, ROBESCU MS, LICASTRO E, TEDESCO C, MARTELLO I, MAFFEI L, VINCENTI G, BAVARO T, COLLINA S. Biocatalysis: a smart and green tool for the preparation of chiral drugs[J]. *Chirality*, 2022, 34(11): 1403-1418.
- [14] WIDERSTEN M, GURELL A, LINDBERG D. Structure-function relationships of epoxide hydrolases and their potential use in biocatalysis[J]. *Biochimica et Biophysica Acta*, 2010, 1800(3): 316-326.
- [15] GODASE VP, KUMBHAR NM, GOVINDWAR SP, RAVI KUMAR A. Characterization reveals a putative epoxide hydrolase from *Yarrowia lipolytica* with the ability to convert rac-1,2-epoxyhexane to (*R*)-diol[J]. *Process Biochemistry*, 2023, 125: 248-258.
- [16] BUČKO M, KANIAKOVÁ K, HRONSKÁ H, GEMEINER P, ROSENBERG M. Epoxide hydrolases: multipotential biocatalysts[J]. *International Journal of Molecular Sciences*, 2023, 24(8): 7334.
- [17] ZOU JY, HALLBERG BM, BERGFORS T, OESCH F, ARAND M, MOWBRAY SL, JONES TA. Structure of *Aspergillus niger* epoxide hydrolase at 1.8 Å resolution: implications for the structure and function of the mammalian microsomal class of epoxide hydrolases[J]. *Structure*, 2000, 8(2): 111-122.
- [18] CHOI WJ, CHOI CY. Production of chiral epoxides: epoxide hydrolase-catalyzed enantioselective hydrolysis[J]. *Biotechnology and Bioprocess Engineering*, 2005, 10(3): 167-179.
- [19] HUANG R, LI C, ZHAO SG, LIU QT, LIU Y, XUE ZL. Enantioconvergent hydrolysis of racemic 1,2-epoxypentane and 1,2-epoxyhexane by an engineered *Escherichia coli* strain overexpressing a novel *Streptomyces fradiae* epoxide hydrolase[J]. *Enzyme and Microbial Technology*, 2023, 166: 110228.
- [20] ZOCHER F, ENZELBERGER MM, BORNSCHEUER UT, HAUER B, SCHMID RD. A colorimetric assay suitable for screening epoxide hydrolase activity[J]. *Analytica Chimica Acta*, 1999, 391(3): 345-351.
- [21] MATEO C, ARCHELAS A, FURSTOSS R. A spectrophotometric assay for measuring and detecting an epoxide hydrolase activity[J]. *Analytical Biochemistry*, 2003, 314(1): 135-141.

- [22] HOLMQUIST M. Alpha/beta-hydrolase fold enzymes: structures, functions and mechanisms[J]. *Current Protein & Peptide Science*, 2000, 1(2): 209-235.
- [23] KUAN J, TSAI CH, CHOU CC, WU C, WU WF. Enzymatic characterization of a novel HSL family IV esterase EstD04 from *Pseudomonas* sp. D01 in mealworm gut microbiota[J]. *Molecules*, 2023, 28(14): 5410.
- [24] STOJANOVSKI G, DOBRIJEVIC D, HAILES HC, WARD JM. Identification and catalytic properties of new epoxide hydrolases from the genomic data of soil bacteria[J]. *Enzyme and Microbial Technology*, 2020, 139: 109592.
- [25] BELOTI LL, COSTA BZ, TOLEDO MAS, SANTOS CA, CRUCELLO A, FÁVARO MT, SANTIAGO AS, MENDES JS, MARSAIOLI AJ, SOUZA AP. A novel and enantioselective epoxide hydrolase from *Aspergillus brasiliensis* CCT 1435: purification and characterization[J]. *Protein Expression and Purification*, 2013, 91(2): 175-183.
- [26] XU W, XU JH, PAN J, GU Q, WU XY. Enantioconvergent hydrolysis of styrene epoxides by newly discovered epoxide hydrolases in mung bean[J]. *Organic Letters*, 2006, 8(8): 1737-40.
- [27] VAN LOO B, KINGMA J, ARAND M, WUBBOLTS MG, JANSSEN DB. Diversity and biocatalytic potential of epoxide hydrolases identified by genome analysis[J]. *Applied and Environmental Microbiology*, 2006, 72(4): 2905-2917.
- [28] JIN HX, LI Y, ZHANG QW, LIN SJ, YANG ZS, DING GF. Enantioselective hydrolysis of styrene oxide and benzyl glycidyl ether by a variant of epoxide hydrolase from *Agromyces mediolanus*[J]. *Marine Drugs*, 2019, 17(6): 367.
- [29] ZOU SP, ZHENG YG, WU Q, WANG ZC, XUE YP, LIU ZQ. Enhanced catalytic efficiency and enantioselectivity of epoxide hydrolase from *Agrobacterium radiobacter* AD1 by iterative saturation mutagenesis for (*R*)-epichlorohydrin synthesis[J]. *Applied Microbiology and Biotechnology*, 2018, 102(2): 733-742.
- [30] HU D, TANG CD, LI C, KAN TT, SHI XL, FENG L, WU MC. Stereoselective hydrolysis of epoxides by reVrEH3, a novel *Vigna radiata* epoxide hydrolase with high enantioselectivity or high and complementary regioselectivity[J]. *Journal of Agricultural and Food Chemistry*, 2017, 65(45): 9861-9870.
- [31] SAINI P, KUMAR N, WANI SI, SHARMA S, CHIMNI SS, SAREEN D. Bioresolution of racemic phenyl glycidyl ether by a putative recombinant epoxide hydrolase from *Streptomyces griseus* NBRC 13350[J]. *World Journal of Microbiology & Biotechnology*, 2017, 33(5): 82.
- [32] HU D, WANG R, SHI XL, YE HH, WU Q, WU MC, CHU JJ. Kinetic resolution of racemic styrene oxide at a high concentration by recombinant *Aspergillus usami* epoxide hydrolase in an *n*-hexanol/buffer biphasic system[J]. *Journal of Biotechnology*, 2016, 236: 152-158.
- [33] XUE F, LIU ZQ, ZOU SP, WAN NW, ZHU WY, ZHU Q, ZHENG YG. A novel enantioselective epoxide hydrolase from *Agromyces mediolanus* ZJB120203: cloning, characterization and application[J]. *Process Biochemistry*, 2014, 49(3): 409-417.
- [34] WU SK, LI AT, CHIN YS, LI Z. Enantioselective hydrolysis of racemic and *Meso*-epoxides with recombinant *Escherichia coli* expressing epoxide hydrolase from *Sphingomonas* sp. HXN-200: preparation of epoxides and vicinal diols in high *ee* and high concentration[J]. *ACS Catalysis*, 2013, 3(4): 752-759.
- [35] JANSON G, PAIARDINI A. PyMod 3: a complete suite for structural bioinformatics in PyMOL[J]. *Bioinformatics*, 2020, 37(10): 1471-1472.
- [36] CLEMENTEL D, del CONTE A, MONZON AM, CAMAGNI GF, MINERVINI G, PIOVESAN D, TOSATTO SCE. RING 3.0: fast generation of probabilistic residue interaction networks from structural ensembles[J]. *Nucleic Acids Research*, 2022, 50(W1): W651-W656.